

Reciprocal Translation between SAR and Optical Remote Sensing Images with Cascaded-Residual Adversarial Networks

Shilei Fu, *Student Member, IEEE*, Feng Xu, *Senior Member, IEEE* and Ya-Qiu Jin, *Life Fellow, IEEE*

Abstract—Despite the advantages of all-weather and all-day high-resolution imaging, synthetic aperture radar (SAR) images are much less viewed and used by general people because human vision is not adapted to microwave scattering phenomenon. However, expert interpreters can be trained by comparing side-by-side SAR and optical images to learn the mapping rules from SAR to optical. This paper attempts to develop machine intelligence that are trainable with large-volume co-registered SAR and optical images to translate SAR image to optical version for assisted SAR image interpretation. Reciprocal SAR-Optical image translation is a challenging task because it's raw data translation between two physically very different sensing modalities. This paper proposes a novel reciprocal adversarial network scheme where cascaded residual connections and hybrid L1-GAN loss are employed. It is trained and tested on both spaceborne GF-3 and airborne UAVSAR images. Results are presented for datasets of different resolutions and polarizations and compared with other state-of-the-art methods. The Fréchet inception distance is used to quantitatively evaluate the translation performance. The possibility of unsupervised learning with unpaired SAR and optical images is also explored. Results show that the proposed translation network works well under many scenarios and it could potentially be used for assisted SAR interpretation.

Index Terms—Synthetic aperture radar, generative adversarial network (GAN), image translation, cascaded residual connection, Fréchet inception distance

I. INTRODUCTION

SYNTHETIC Aperture Radar (SAR) is capable of imaging at high resolution in all-day and all-weather conditions. As a cutting-edge technology for space remote sensing, it has found wide applications in earth science, weather change, environmental system monitoring, and marine resource

utilization, planetary exploration and etc. Space-borne SAR technology has advanced greatly since 1970's. New imaging modalities and novel constellation concepts are under development [e.g. 1-4]. Despite the rapid progresses in SAR imaging technologies, the challenge still remains in the interpretation of SAR imagery and it is becoming more and more urgent as a huge volume of SAR data is being acquired daily by numerous radar satellites in orbits.

Due to its distinct imaging mechanism and the complex electromagnetic (EM) wave scattering process, SAR exhibits very different imaging features from optical images. Some basic differences between SAR images and natural optical images are summarized in Table I. Human's visual system is adapted to the interpretation of optical images. SAR image is difficult to interpret by ordinary people. Although SAR images contain rich information about target and scene, such as geometric structure and material property, they can only be interpreted by well-trained experts. This has now become the major hindrance in utilization of existing SAR archives and further promotion of SAR applications.

Experts of SAR imagery interpretation are often trained by comparing the SAR image side-by-side with the corresponding optical image (e.g. Fig. 1). From such SAR-vs-Optical comparison experiences, experts conclude useful rules which translate between features in SAR and optical remote sensing images. Thereafter, they are able to direct interpret a new image from similar SAR sensors. Ideally, such training could be done in computers with artificial intelligence (AI) by leveraging the recent progresses in AI and deep learning technologies.

The major objective of this work is to develop machine learning algorithm which is trainable with large amount of co-registered SAR and optical images to translate from SAR image to optical images and vice versa. The translated optical image can then be used in assisted interpretation of SAR image by ordinary people. Imagine that, with such translation tool, any person without any background knowledge of radar, could be able to understand SAR image. This could greatly promote the wide application and usage of future and existing archive of SAR remote sensing imagery. Other potential applications include facilitation of data fusion of optical and SAR images, e.g. translating optical image at an earlier date as the reference SAR image for SAR change detection, registering the unpaired SAR and optical images, integrating optical and microwave data into a single image to enhance earth surface features etc.

This paragraph of the first footnote will contain the date on which you submitted your paper for review.

This work was supported in part by National Key R&D Program of China no. 2017YFB0502703 and Natural Science Foundation of China no. 61822107, 61571134."

The authors are with the Key Laboratory for Information Science of Electromagnetic Waves (MoE), Fudan University, Shanghai, China 200433 (e-mail: fengxu@fudan.edu.cn).

Deep learning, in particular convolutional neural networks (CNNs), have revolutionized the computer vision regime since the first successful application of CNN in practical image classification task in 2012 [27]. It utilized stacked convolution and pooling layers to automatically extract features at different scales via supervised learning. Since 2014, CNN-based approaches have been applied in interpretation of SAR images [28], including the typical tasks such as automatic target recognition (ATR) [7][29], earth surface classification [1][30], speckle reduction [31], change detection [36], etc.

Generative adversarial networks (GANs) [17] are a special type of CNNs which are often used to generate synthesized images using actor-critic scheme. It simultaneously trains a generative CNN, the ‘actor’, which tries to generate images as realistic as possible, and a discriminative CNN, the ‘critic’, which tries to identify the synthesized images from the real images. Some relevant works which employed GAN-like approaches to analyze SAR images are reviewed in subsection II-A.

On the other hand, image translation itself is an interesting problem in computer vision. Some interesting approaches in this regard are reviewed in subsection II-B. Most of these image translation studies deal with the problem of style transfer where the objective is change the style of image, e.g. from optical to cartoon picture, or from semantic map to optical picture. Only one end of the translation is raw sensor data.

However, the problem of translation between SAR and optical images are more complicated. It involves with two distinct types of raw sensor data. Table I lists several major differences of SAR and optical imaging mechanisms and the corresponding distinct phenomena. As a result, the information content in SAR and optical image are partial overlapped and partial exclusive, which means that only part information is observed by both sensors and each sensor observes information that is not observable by the other sensor. A successful translation algorithm should be able to convert the common part of information content from one sensing modality to the other, and ideally, generate the new information content from learned experiences. Some earlier attempts in SAR-optical fusion [37] suggested that existing state-of-the-art translation GANs are not able to direct translate from SAR to optical images (see subsection II-C). We believe that such cross-modality raw data translation requires a novel and fine-tuned network scheme and a large volume of co-registered image pairs as training data.

To demonstrate the challenge in translating across the two sensing modalities, Fig. 1 gives four example image pairs, i.e. low-rise buildings, high-rise buildings, waters and roads. The differences between SAR and optical images are marked in red circles. For low-rise buildings, the gap between houses cannot be distinguished in SAR images. For high-rise buildings, the projection directions of buildings differ in the two sensing modalities. And buildings in SAR images scatter heavily and have severe layover effect with nearby buildings. For waters, ripples in optical images may not appear in SAR images. For roads, small roads are not nearly noticeable in SAR images due to layovers and shadows.

In this paper, we propose a novel SAR-Optical image reciprocal translation GAN architecture. It employs a CNN as the discriminator and a specially-designed network as the generator (translator). The translator uses the multi-scale encoder-decoder CNN as the backbone and incorporates novel multi-scale cascaded-residual connections. The GAN is trained alternatively in a min-max fashion. The discriminator is trained to maximize the difference between the co-registered generated sample and true sample, while the translator is trained to minimize it. To reduce the instability during the training of GAN, a hybrid loss function is used to train the generator which contains two parts: the GAN loss back-propagated from discriminator output, and the L1-distance loss directly applied to the generated sample and true sample.

The proposed method is verified on a large volume SAR-Optical image pairs, i.e. ~ 10000 samples of 256×256 size patch. The dataset covers 5 different urban/suburban regions and mainly contains earth surfaces such as built-up areas, roads, vegetation, waters and farmlands. Appearances of these terrain objects, e.g. buildings, have great diversity which makes the training and testing more generalizable. The algorithm is tested at different resolutions. The Fréchet inception distance (FID) [8] is used as the quantitative measure of the similarity between the reconstructed and the true image. For low-resolution (6m, 10m), the reconstructed result appears to be very similar and the FID indicates very high similarity. For high-resolution (0.5m), the reconstructed result appears to be reasonable but not exactly captures the fine geometric features of manmade objects such as buildings and roads. This indicates that the mutual-exclusive part of information content in two sensing modalities becomes significant at higher resolutions. Overall, the translated high resolution optical image can partially serve the purpose of assisted interpretation of SAR images.

The major contributions of this paper are as follows

- 1) A novel image translation network architecture is proposed for raw image translation between two very different sensing modalities, SAR and optical sensor. Two critical innovations are the cascaded residual connections in the translator network and the L1+GAN hybrid loss function. Evaluation results on large volume of dataset demonstrate good visual quality and variety.
- 2) Extensive analyses are conducted with quantitative metrics (e.g. FID) on the proposed approach with space-borne and airborne SAR images. It is compared with existing image translation methods. Different factors are analyzed including resolutions, targets, polarization, frequency bands, input image scales etc.
- 3) An extension towards unsupervised learning is proposed with cyclic training loops. Results demonstrate that using large-volume of unpaired SAR and optical images, the performance can be further improved.

This paper is organized as follows. Section II reviews the relevant recent studies about image translation and SAR generation. Section III presents the proposed translation network architecture, loss function and training techniques. Experiments with real SAR images are carried out and results are presented and evaluated in Section IV. Finally in Section V,

conclusions are drawn and the future perspectives of application are discussed.

II. RELATED WORKS

A. GAN in SAR Image Analysis

GAN or general generative neural networks have been applied in various tasks in SAR image analysis. For instance, Song et al. [7] proposed zero-shot learning scheme for SAR ATR which is able to extract target orientation and orientation-invariant intrinsic features via training SAR generative networks. Pan et al. [38] proposed a novel super-resolution method namely dense residual GAN and utilized the memory mechanism to extract hierarchical features for better reconstruction of remote sensing images. Guo et al. [32] employed GAN to synthesize the desired SAR images according to angle information and its feasibility was validated by comparison with real images and ray-tracing results. Gao et al. [34] introduced the multi-classifier to the discriminator so that the images' labels of the Moving and Stationary Target Acquisition and Recognition (MSTAR) were made the most of to synthesize realistic SAR targets.

B. Image Translation

Image translation is conversion between two types of images. It constructs an intermediate latent space, which maps the two image fields X_1, X_2 to the latent space Z through two encoders and then reconstructs X_2, X_1 respectively through decoders [10]. Currently, the mainstream image translation methods are based on GANs. Compared with traditional loss functions such as L2 and L1 norms, GANs can generate sharper and more realistic images.

Slightly different from conventional GANs, image translation networks are conditional GANs [11] and require the original image as input. Existing studies of image translation can be mainly divided into two categories.

The first category employs end-to-end image mapping strategy which directly converts the original image to the translated domain. Taigman et al. [25] translated optical images to cartoon images using the domain transfer network. Isola et al. [9] proposed the Pix2Pix network to translate optical aerial image to maps. It is based on U-Net architecture [24]. Liu et al. [10] proposed CycleGAN for image translation, which addresses the mode collapse issue of GAN by introducing cyclic mechanism involving self-reconstruction, image translation and cyclic reconstruction. Similar studies include Chen et al. [16] synthesized photographic urban scenes with semantic segmentation maps using a cascaded refinement networks. Zhu et al. [26] changed the properties of targets in the images, such as the animal categories and the seasons of the scenes.

The second category employs the style transfer strategy. It assumes that the images in two different domains share the same large-scale features, but have distinct small-scale features. Thus, it first separates the style from the contents of images and then replaces the style of the original image with the translated

style. It assumes that the contents of an image are conveyed in the low-frequency large-scale edges while the styles are represented by the high-frequency small-scale textures. Gatys et al. [13] proposed the Gram Matrix, the correlation coefficient matrix between each feature maps as extracted by CNNs, to represent the style of images. John et al. [14] trained a feed-forward network to solve the optimization problem proposed by Gatys in real-time rather than adjusting the input according to the target. FaderNets, proposed by Lample et al. [15], trained the discriminator to disentangle some specific style attributes and invariant intrinsic features from the encoded representation.

C. Fusion of SAR and Optical Images

Many works have been carried out in the multi-sensor image fusion regime [12]. The main objective of data fusion is to integrate complementary information from multi-sensor images of the same region into an enhanced image which appears better than any of the original ones. Hybrid pansharpening method, the weighted combination method (WC method), the integration method (MR method) based on the magnitude ratio of the two images are often employed. The fused images are well-defined and diversely textured. Garzelli et al. [22] leveraged co-registered SAR image to improve the quality of optical images, which extracts information from SAR image and complements with optical image so that the targets could appear clearer.

Another type of fusion work is SAR and optical image registration. The focus is to explore the consistent features between the two sensing modalities. Fan et al. [33] designed a uniform nonlinear diffusion-based Harris feature extraction method to explore many more well-distributed feature points with potential of being correctly matched. Liu et al. [36] transformed the two types of images into a feature space where their feature representations became more consistent using a deep convolutional coupling network. Nina et al. [37] synthesized artificial SAR-like patches from optical images and matched them with the true SAR patches utilizing NCC, SIFT or BRISK. Especially, the second method is very instructive for the consistence of the feature space in the SAR and optical image translation.

A third type of fusion is to combine multi-temporal SAR and optical image to generate images of different observation time. He et al. [35] used a conventional conditional GAN to generate the optical images from optical images at a different date with the aid of a SAR image acquired at the both dates. It also tried to directly generate optical image from a single SAR image but found that the existing GANs failed to do so.

III. SAR-OPTICAL RECIPROCAL TRANSLATION NETWORK

A. Translation Framework

The proposed framework is shown in Fig. 2. It has two reciprocal directions of translation, i.e. SAR to Optical and Optical to SAR. Each direction consists of two adversarial deep networks, i.e. a multi-scale convolutional encoder-and-decoder

network as the translator (generator) vs. a convolutional network as the discriminator. The translator takes in SAR image, maps it to the latent space via the encoder, and then remaps it to a translated optical image. The discriminator takes in both the translated optical image and the true optical image which is co-registered with the original SAR image, and outputs the classification results. The discriminator learns to identify the translated optical images from the true optical images, while the translator network learns to convert the SAR image to an optical image as realistic as possible to fool the discriminator. On the other direction, the network is constructed exactly in the same manner with the only difference being optical as input and SAR as translated image.

The discriminator is a conventional CNN for binary classification task. The translator has multi-scale convolutional layers for encoder and decoder where direct paths are connected from the encoder to the decoder at different scales. Beside the direct paths in the latent space, residual connections in the input image space are further incorporated at each scales. A conventional binary classification loss is employed to train the discriminator, while its opposite loss, together with a L1 norm loss, are used to train the translator. These are explained in detail in the following subsections.

B. Network Architecture

Fig. 3 shows the architecture and parameters of the translator network. On the encoder side, the input image is convolved at one scale and downsampled to the next scale repeatedly for 12 times. On the decoder side, the latent feature map is deconvolved and upsampled back to the original scales. Following the U-net structure [24], we include direct links in the latent space from encoder to decoder. In addition, the input image is downsampled accordingly to different scales and a residual link is added from encoder to decoder. For the residual links, the downsampled inputs are attached (but not added) to the feature maps in the decoders. Such multi-scale residual connections have been proved to be effective in generating high-resolution images [16][20][21]. In order to increase the depth of the network, at each time upsampling the feature maps, it first concatenate the encoder's feature maps to the current ones and deconvolve. Then concatenate the residual block to the former output feature maps and deconvolve again. This results in the increase of the decoder's receptive field. Thus the receptive field of the encoder and that of the decoder will be asymmetrical, which may degrade performance. The solution is to convolve feature maps of each scale twice in the encoder.

Regarding the hyper-parameters, in the translator, the convolutional kernel is 3×3 , the encoder and the decoder each have 12 layers, and the receptive field per pixel of the input image is 191×191 . In the discriminator, the kernel is 4×4 , and it has 5 layers and the receptive field is 70×70 . The benchmark number of feature maps in the generator is set to 50. The number of feature maps doubles at each downsampling and diminishes double after each upsampling. Those in the discriminator are respectively 64, 128, 256, 512 and 1. That means in the discriminator, the feature maps extracted from the

input image are finally mapped into a 32×32 matrix and every value corresponds to a 70×70 patch of the input. By contrast, the difference between the discriminative matrix of the true image and that of the reconstructed image could determine how similar are the spatial structure of the two images. The total number of the generator's weights is approximately 53.75 million and that of the discriminator is 2.76 million. The network architectures are depicted in detail in Fig. 3 and Fig. 4.

C. Loss Function

Loss functions are critical for training of the networks. The discriminator is trained with a binary classification log-loss, i.e.

$$L(D) = -E_{x \sim p_{data}(i)} [\log D(x)] - E_{z \sim p_{data}(j)} [\log (1 - D(T(z)))] \quad (1)$$

where $i = 0, 1$ in $p_{data}(i)$ demonstrate the distributions of the true optical and SAR images respectively. $E_{x \sim p_{data}(i)}$ denotes that x obeys the distribution $p_{data}(i)$, and $E_{z \sim p_{data}(j)}$ denotes that z obeys the distribution $p_{data}(j)$. When z denotes the original input SAR (or optical) image, $T(z)$ denotes the translated optical (or SAR) image and x denotes the corresponding true optical (or SAR) image. $D(\cdot)$ denotes the output probability map of the discriminator. For the discriminator, minimizing $L(D)$ is equivalent to classifying x as 1 and $T(z)$ as 0.

Following the adversary scheme, the loss function of the translator is

$$L_{GAN}(T) = - \sum_i E_{z \sim p_{data}(i)} [\log (D(T(z)))] \quad (2)$$

where $L_{GAN}(T)$ is the sum loss of the two translated networks. Opposite to the goal of the discriminator, the translator is aimed at synthesizing 'realistic' images to fool the discriminator to classify them as 1.

It is found that the adversary loss function is better to be hybrid with traditional loss, such as L1 or L2 loss [9]. Our experiments indicate that L2 loss results in blurred images. Therefore, L1 norm loss is used to hybrid with the GAN loss, i.e. L1 distance between the translated image $T(z)$ and the true image x :

$$L_{L1}(T) = \sum_{i,j} E_{x \sim p_{data}(i), z \sim p_{data}(j)} [\|x - T(z)\|_1] \quad (3)$$

Combine the above two equations together with appropriate weights and derive the final loss function $L(T)$ of the translators.

$$L(T) = L_{GAN}(T) + \beta L_{L1}(T) \quad (4)$$

$L(T)$ is the objective function for two translators, whose parameters are simultaneously updated. The two discriminators are allocated with the independent loss function $L(D)$ and trained separately.

A quick experiment is conducted to show the efficacy of proposed loss function. Different losses contribute differently to the qualities of reconstructed results. In Fig. 5, it is found that reconstructed images trained under L1-only loss are blurred and low-frequency features such as contours can be learned

while high-frequency fine textures are missing. The model trained under GAN-only loss can learn the details and the targets are more prominent, but large-scale smooth features and their spatial distributions are not well reconstructed. We also notice that some artifacts appear in homogenous areas such as water. Besides, training with GAN-only loss often encounters the well-known ‘mode collapse’ problem [39]. Mode collapse is a fatal training problem of GAN where $T(z)$ is collapsed to a fixed sample to maintain low loss but sacrificing the diversity. These issues can be avoided by using the proposed hybrid L1 and GAN loss, in which case, the synthesized images can have both low-frequency and high-frequency characteristics. Moreover, the network can also be trained more stably with the hybrid loss.

D. Training Strategy

Stochastic gradient descent algorithm with adaptive moment estimation can be used to train the two translators/discriminators simultaneously. Following GAN training strategy, one iteration consists of the following step (see Fig. 6):

- a) Forward Pass – Weights of translators and discriminators are randomly initialized. A mini-batch of SAR images are then sent to the translator A to synthesize fake optical images, while a mini-batch of optical images are sent to the translator B to synthesize fake SAR images. Next, the fake and real optical images are sequentially sent to the same discriminator A, which generates two probability maps respectively. The fake and real SAR images are sent to the discriminator B and the discriminator B also generates corresponding probability maps.
- b) Backward Pass – The two probability maps of optical images are compared in the loss to optimize the discriminator A, while those of SAR images are compared to optimize the discriminator B. The sigmoid function is selected as the activation function for the discriminator, which functions as a binary classifier. The discriminator is trained to distinguish the fake as 0 and the real as 1. The discriminator classifies the image patches separately. This not only limits the receptive field, but also provides more samples for the training [23]. Both of the two losses are also added as the GAN loss for the translators, which have to maximize them. That means the aim of both the translators is to generate sufficiently-realistic images to fool the discriminators. The real and fake ones are also compared directly to ensure the positional mappings of targets are correct. Thus, the joint losses are applied as the final loss function of the two translators. Then the backpropagation is applied to adjust the trainable parameters in the two translators simultaneously.

The forward process alternates with the backward process. The batch size is set as 1. The technique of GPU parallel acceleration with 4 Titan X is employed, which means four pairs of SAR and optical images are used to train the network each time simultaneously. After the gradients of the four threads are all calculated, the mean gradients are used to update the optimizers. The backward pass is a single thread. After

finishing the back propagation, another four pairs of images are sent in. Traversing all the images is considered as an epoch. Then reshuffle the images and traverse next epoch.

The parameter in Eq. (4) is set as $\beta = 20$. We set the learning rate to 0.0002. Adam optimizer with $\beta_1=0.5$ is used. The input images are linearly mapped to the interval $[-1,1]$. Leaky ReLU is selected as the activation function. Batch normalization is used before the activation function except the first or last layer. All the trainable parameters are initialized as the truncated normal distribution with mean 0 and standard deviation 0.02. When the batch size is set too small, due to the difference between training samples, a slight oscillation occurs in the gradient decent and the curve of the loss convergence appears steady declining with oscillations. Early stop is adopted during training. When the training loss does not decrease for four epochs in a row, the training is forced to stop.

In terms of training time, it takes only about 0.4 second per batch and 18 minutes to run through an epoch (10284 pairs of samples). Another 3 minutes are needed to test the test samples and save the test results and the checkpoint of the model. So it costs around 21 minutes to finish training and testing for an epoch.

E. Towards Unsupervised Learning

Supervised learning with well co-registered optical and SAR image pairs produces good results. However, such dataset is not always available and even available, would require a significant amount of effort for image registration. Thus, this paper also explores the possibility of unsupervised learning with unpaired SAR and optical images. CycleGAN [26] proposes a cyclic loop which could be leveraged for this purpose. As shown in Fig. 7, the SAR image is first fed to the translator A and synthesizes fake optical image. Then the fake optical image is used to synthesize the cyclic fake SAR images by the translator B. On the other hand, the optical image is used to synthesize fake SAR image which is then further used to synthesize the cyclic fake optical images. The cyclic images are compared with the corresponding true image in a pixel-by-pixel fashion, while the synthesized fake images are fed into the ‘critic’ discriminator networks. The translator A and translator B networks are trained alternatively during these two loops together with the discriminator networks. Later in subsection IV-E, we demonstrate how such unsupervised learning could further improve the performance of a translator initially trained with small number of co-registered image pairs.

IV. EXPERIMENTS AND ANALYSES

A. Datasets

SAR data used in this study mainly comes from the spaceborne GF3 SAR from China [40] and the airborne UAVSAR system from NASA [41]. The information of those data used in our experiments is listed in the following Table II.

UAVSAR (Uninhabited Airborne Vehicle Synthetic Aperture Radar) radar system is an L-band polarimetric instrument developed by NASA. As shown in Fig. 8, UAVSAR

data used here mainly consists of five types of earth surfaces, buildings, vegetation (mountains are usually covered with trees and classified as vegetation), farmlands, waters and deserts. It has pixel resolution of about $6.2407\text{m} \times 4.9156\text{m}$.

GF3 satellite is China's first C-band multi-polarization SAR satellite. Two large scenes of GF3 images are used in the study with a resolution of 0.51m. The dataset contains different urban/suburban regions. In Fig. 9, the GF3 SAR image after geocoding is shown on the left. It mainly contains five terrain surfaces, i.e. buildings, roads (highways or overpass), vegetation, waters (lakes, rivers or seas) and farmlands. Buildings can be further divided into low-rise and high-rise buildings.

A simple preprocessing step is applied to adjust the grayscale of the SAR image by limiting the minimum and maximum gray levels. Another preprocessing step is to perform speckle filtering on the SAR images using a fast nonlocal despeckling filter [42]. We found that speckle filtering can improve the quality of the final synthesized images. The training samples are 256×256 patches cropped from the large SAR and optical images. We have a total of 12854 pairs of co-registered samples, 20% of which are randomly selected as test samples while the rest as training samples. During the preparation of the dataset, it is found that, due to the difference of acquisition time of SAR and optical images, some new buildings shown in the recent optical images were not captured in the SAR image. This may adversely affect the final results.

B. Quantitative Evaluation

Here we design experiments to test the performance of our model for SAR images of different resolutions and different polarization modes. The experiment for different resolutions adopts medium resolution UAVSAR and high resolution GF3 datasets respectively; the experiment for different polarization modes uses single-polarized and full-polarized UAVSAR data.

1) Resolution

The UAVSAR images are resampled to resolution of 6m and 10m and then used to train the proposed network. An example of translated SAR and optical images are shown in Fig. 10 where a good visual quality is achieved.

Fig. 11 shows examples of high-resolution GF3 images translated by the proposed networks. The first row is a training sample and the rest three rows are test samples. It is found that earth surfaces like waters and vegetation can be easily reconstructed in both training and test cases. Low-rise buildings can be rebuilt into cubes, but their edges are not well-aligned. If the buildings are too close, the open space between them is difficult to distinguish. For high-rise buildings, the ones shown in the training sample appear to be reasonably realistic. However, the ones in the test sample in the bottom row appear to be smeared. It seems like that the network got confused by the viewing angles. Apparently, for tall 3D terrain objects, both SAR and optical images are very sensitive to the view angles. Without incorporation of the projection mechanism, the proposed network is not able to generalize in this dimension.

It is necessary to quantitatively measure the difference between the translated images and true ones. Traditional methods, such as L1, Peak Signal-to-Noise Ratio (PSNR) and Structural Similarity Index (SSIM) [19], could be used to measure the similarity between two images. However, these methods still compare the similarity in terms of pixel values but rather than in the sense of perceptual similarity. Inception score (IS) [18] and Fréchet inception distance (FID) [8] are usually used to quantitatively evaluate the quality and variety of images generated by GANs. As shown in Fig. 12, both of them encode the input image to a feature vector by using the inception network, which functions as the human visual perception. If the two images are identical, their encoded feature vectors should be the same.

Different from IS, FID uses the statistics of real world samples and compares them to the statistics of synthetic samples. FID between the Gaussian distribution with mean and covariance (m_1, C_1) and the Gaussian distribution with (m_2, C_2) is defined as $\|m_1 - m_2\|_2^2 + \text{Tr}(C_1 + C_2 - 2(C_1 C_2)^{1/2})$. Lower FID is better, corresponding to more similar real and generated samples. It is found that the FIDs of the generated 0.51m optical and SAR images are respectively 154.7532 and 53.0067. The values are quite large, which indicates that the model performs badly. However, the reconstructed images are very good from the perspective of human eye. The buildings, farmlands, green areas, etc. in each image are generally well classified. The textures are also allocated. Nevertheless, an exception exists. The textures of buildings vary widely and are hard to match one-to-one with ground truths. For large-scale urban scenes, high-frequency parts such as noise and details in ground truths are difficult to learn because those in each sample differ greatly. Our main purpose is to reconstruct their main contours.

The number of samples to calculate the Gaussian statistics (mean and covariance) should be greater than the dimension of the last coding layer, here 2048 for the inception pool 3 layer [8]. Otherwise the covariance is not full rank, which will result in complex numbers and nans by calculating the square root. Here, we use 2048 pairs of test samples to calculate the FID to estimate the capability of the generators.

Table III lists the tested FID values for the different resolution datasets mentioned above. Randomly select 2048 pairs of samples from each dataset and calculate the corresponding FID value. Repeat three times and use the mean as the ability of our model to train this kind of dataset. It indicates that 6m data performs better than 0.51m and 10m data. The 10m results are not ideal due to their small features hard to extract.

Note that FID could be further reduced by increasing the number of samples. As shown in Table IV for the case of 6m full-pol UAVSAR, its FID could be reduced to 72 for optical and 42 for SAR if given 10000 samples.

2) Polarization

So far, the used SAR data is all HH or VV single-pol. Full-pol data contains rich polarimetric information. It is worth to investigate how the performance might improve if full-pol

SAR is used. For simplicity, the pauli color-coded image is used as an proxy of full-pol SAR data. We carry out an experiment to train our model with full-pol images and single-pol images in the same region respectively, and compare the translation performance. As shown in Table III, it indicates that 6m full-polarized data has the best performance, especially the reconstructed optical images are much better than those from 6m single-pol data.

Four examples of different kinds of earth surfaces, waters, vegetation, farmlands and buildings are shown Fig. 13, respectively. Apparently, the optical images translated from full-pol SAR images are more vivid and realistic than those from single-pol images.

Fig. 14 further investigates into few interesting cases. In each case, one building in single-pol image and the corresponding full-pol image is marked correspondingly in each row. Note that these buildings are all easily observable in the full-pol image but not in the single-pol image. This is mainly because of the imbalance of scattering power distribution over different polarization channels. The translated optical image appear to be much more realistic and closer to true image. Apparently, it is benefited from the additional rich information conveyed in the full-pol SAR image.

C. Comparison with Existing Translation Networks

To evaluate the performance of the proposed method in the context of existing image translation approaches. Here, we compare it with CycleGAN [10] and Pix2Pix [9] using the 0.51m GF3 images. In order to ensure the fairness of comparison, the discriminators and the receptive fields of the generators are the same. The number of the generators' layers and that of the total trainable parameters are the same. The parameters of the network are randomly initialized. To remove the slight dependence of training result on the initialization, each network is repeatedly trained for 3 times with the same data and then the best result is chosen.

In Fig. 15, four representative pairs of different earth surfaces are selected. It can be found that in the first two rows, the buildings reconstructed by our method are more natural. In the third and fourth rows, waters, roads and vegetation reconstructed by CycleGAN are similar to the proposed method.

In Table V, the three metrics PSNR, SSIM and FID are all employed. PSNR and SSIM analyze the statistical distribution of pixel values. The smaller the FID, or the larger the PSNR and SSIM, the more similar the two datasets are. On the 0.51m dataset, our proposed method outperforms CycleGAN and Pix2Pix in the other three indicators, especially the FID score improved a lot.

D. Generalization to Different SAR Platforms

Generalization capability is critical to make the proposed method applicable in practical scenarios. One key aspect is generalization to different geographic scenes. From the cases presented in previous subsections, the test samples are acquired

from different regions than then training samples, where the low FID has demonstrated that the proposed method can be generalized to different scenes. Another critical test is generalization to different SAR platforms, e.g. a model is trained with data from one SAR platform but used to translate SAR image from another platform.

An experiment is conducted where the model trained using UAVSAR images are used to translate SAR images from UAVSAR, GF3 and ALOS2 acquired at different regions (Fig. 16). Compared to the ground truth, the performance of translation is largely degraded in the case of GF3 and ALOS2. The boundary of different terrain surfaces are smeared. We believe that this is partially attributed to the fact that SAR images from different platforms are not cross-calibrated.

Note that when applied to processing real SAR image, we prefer to process one large image at a time. Although the network is trained and designed to take inputs of 256×256 patches, it is a fully convolutional network and can be directly extended to process larger size images without any modification. Experiments were conducted to verify the performance of the proposed method when used to process large size images.

E. Enhancement with Unsupervised Learning

Finally, we explore the possibility of further refining the network with unsupervised learning. Note that the unsupervised training starts from the network trained with co-registered images. Then we can feed the SAR or optical images to be tested to the network and train them using large volume of unpaired optical or SAR images. Compared with supervised learning, in which only the prior knowledge from pretraining can be utilized, the model of unsupervised learning can also dynamically learn something new from the extended dataset and refine the results through iterations.

The major experimental procedures are as follows.

- 1) Randomly select n pairs of optical and SAR images apart from the dataset to be tested. Ensure that the earth surfaces are evenly distributed (slightly more buildings for its difficulty to be reconstructed).
- 2) Feed the N test SAR images and the n optical images to the unsupervised network, train until the early stop and save the translated optical images.
- 3) Feed the N test optical images and the n SAR images to the unsupervised network, train until the early stop and save the translated SAR images.
- 4) Check the results and quantitatively evaluate them with those by supervised learning.

As shown in Table VI, it indicates that the translation results are greatly improved with unsupervised learning. The results further refined with unsupervised training is shown in Fig. 17, where we can see that the refined results are more vivid and realistic. However, waters in SAR images don't differ from those farmlands greatly, which results in the imperfect reconstruction of waters.

V. CONCLUSION

For the purpose of assisted interpretation of SAR imagery by ordinary people, this paper proposes a novel image translation network architecture based on GAN for reciprocal translation between SAR and optical remote sensing images. In order to evaluate the translated images from the perspective of human visual perception, the quantitative metric FID is employed. For low-resolution (6m, 10m) UAVSAR dataset, the reconstructed images appear very similar to the true data and the corresponding FID is low. For high-resolution (0.51m) GF3 dataset, the reconstructed results appear reasonable but not exactly capture the geometric features of certain built-up objects such as high-rise buildings. Under the same condition, the proposed network outperforms conventional image translation networks such as CycleGAN and Pix2Pix. Results also show that full-pol SAR image is preferable as input for translation because certain objects are not observable in single-pol SAR images. It is also confirmed that the network does not perform well if generalized across different SAR platforms. Finally, we demonstrate that unsupervised learning could further improve the performance of a translator initially trained with small number of co-registered image pairs which points the right direction towards general application of assisted SAR image interpretation.

REFERENCES

- [1] Andrea MONTI GUARNIERI, Fabio ROCCA, Options for continuous radar Earth observations, *SCIENCE CHINA Information Sciences*, Volume 60, Issue 6, 2017, Pages 060301
- [2] Roger M. FUSTER, Marc FERNÁNDEZ USÓN, Antoni BROQUETAS IBARS, Interferometric orbit determination for geostationary satellites, *SCIENCE CHINA Information Sciences*, Volume 60, Issue 6, 2017, Pages 060302
- [3] R. Wang et al., "First bistatic demonstration of digital beamforming in elevation with TerraSAR-X as an illuminator," *IEEE Trans. Geosci. Remote Sens.*, vol. 54, no. 2, pp. 842-849, 2016.
- [4] Li et al., "Focusing the L-band spaceborne bistatic SAR mission data using a modified RD algorithm," Submitted to IEEE TGRS, 2018
- [5] Zhang Z, Wang H, Xu F, et al. Complex-valued convolutional neural network and its application in polarimetric SAR image classification[J]. *IEEE Transactions on Geoscience and Remote Sensing*, 2017, 55(12): 7177-7188.
- [6] Fan J, Wu Y, Li M, et al. SAR and Optical Image Registration Using Nonlinear Diffusion and Phase Congruency Structural Descriptor[J]. *IEEE Transactions on Geoscience and Remote Sensing*, 2018.
- [7] Song Q, Xu F. Zero-shot learning of SAR target feature space with deep generative neural networks[J]. *IEEE Geoscience and Remote Sensing Letters*, 2017, 14(12): 2245-2249.
- [8] Heusel M, Ramsauer H, Unterthiner T, et al. Gans trained by a two time-scale update rule converge to a local nash equilibrium[C]//Advances in Neural Information Processing Systems. 2017: 6626-6637.
- [9] Isola P, Zhu J Y, Zhou T, et al. Image-to-image translation with conditional adversarial networks[J]. *arXiv preprint*, 2017.
- [10] Liu M Y, Breuel T, Kautz J. Unsupervised image-to-image translation networks[C]//Advances in Neural Information Processing Systems. 2017: 700-708.
- [11] Mirza M, Osindero S. Conditional Generative Adversarial Nets[J]. *Computer Science*, 2014:2672-2680.
- [12] Byun Y, Choi J, Han Y. An area-based image fusion scheme for the integration of SAR and optical satellite imagery[J]. *IEEE Journal of Selected Topics in Applied Earth Observations and Remote Sensing*, 2013, 6(5): 2212-2220.
- [13] Gatys L A, Ecker A S, Bethge M. Image style transfer using convolutional neural networks[C]//Computer Vision and Pattern Recognition (CVPR), 2016 IEEE Conference on. IEEE, 2016: 2414-2423.
- [14] Johnson J, Alahi A, Fei-Fei L. Perceptual Losses for Real-Time Style Transfer and Super-Resolution: Supplementary Material[J].
- [15] Lample G, Zeghidour N, Usunier N, et al. Fader networks: Manipulating images by sliding attributes[C]//Advances in Neural Information Processing Systems. 2017: 5969-5978.
- [16] Qifeng Chen, Vladlen Koltun. Photographic Image Synthesis with Cascaded Refinement Networks[J]. 2017:1520-1529.
- [17] Goodfellow I, Pouget-Abadie J, Mirza M, et al. Generative adversarial nets[C]//Advances in neural information processing systems. 2014: 2672-2680.
- [18] Salimans T, Goodfellow I, Zaremba W, et al. Improved techniques for training gans[C]//Advances in Neural Information Processing Systems. 2016: 2234-2242
- [19] Wang Z, Bovik A C, Sheikh H R, et al. Image quality assessment: from error visibility to structural similarity[J]. *IEEE transactions on image processing*, 2004, 13(4): 600-612.
- [20] Makhzani A, Shlens J, Jaitly N, et al. Adversarial Autoencoders[J]. *Computer Science*, 2015.
- [21] E. L. Denton, S. Chintala, R. Fergus et al., "Deep generative image models using a laplacian pyramid of adversarial networks," in *Advances in Neural Information Processing Systems*, 2015, pp. 1486-1494.
- [22] Garzelli A. Wavelet-based fusion of optical and SAR image data over urban area[J]. *International Archives of Photogrammetry Remote Sensing and Spatial Information Sciences*, 2002, 34(3/B): 59-62.
- [23] Shrivastava A, Pfister T, Tuzel O, et al. Learning from Simulated and Unsupervised Images through Adversarial Training[J]. 2017.
- [24] Ronneberger O, Fischer P, Brox T. U-Net: Convolutional Networks for Biomedical Image Segmentation[C]// International Conference on Medical Image Computing & Computer-assisted Intervention. 2015.
- [25] Taigman Y, Polyak A, Wolf L. Unsupervised Cross-Domain Image Generation[J]. 2016.
- [26] Zhu J Y, Park T, Isola P, et al. Unpaired Image-to-Image Translation using Cycle-Consistent Adversarial Networks[J]. 2017.
- [27] Krizhevsky A, Sutskever I, Hinton G E. Imagenet classification with deep convolutional neural networks[C]//Advances in neural information processing systems. 2012: 1097-1105.
- [28] Zhu X X, Tuia D, Mou L, et al. Deep learning in remote sensing: a comprehensive review and list of resources[J]. *IEEE Geoscience and Remote Sensing Magazine*, 2017, 5(4): 8-36.
- [29] Chen S, Wang H, Xu F, et al. Target classification using the deep convolutional networks for SAR images[J]. *IEEE Transactions on Geoscience and Remote Sensing*, 2016, 54(8): 4806-4817.
- [30] Zhou Y, Wang H, Xu F, et al. Polarimetric SAR image classification using deep convolutional neural networks[J]. *IEEE Geoscience and Remote Sensing Letters*, 2016, 13(12): 1935-1939.
- [31] Yue D X, Xu F, Jin Y Q. SAR despeckling neural network with logarithmic convolutional product model[J]. *International Journal of Remote Sensing*, 2018, 39(21): 7483-7505.
- [32] Guo J, Lei B, Ding C, et al. Synthetic aperture radar image synthesis by using generative adversarial nets[J]. *IEEE Geoscience and Remote Sensing Letters*, 2017, 14(7): 1111-1115.
- [33] Fan J, Wu Y, Li M, et al. SAR and Optical Image Registration Using Nonlinear Diffusion and Phase Congruency Structural Descriptor[J]. *IEEE Transactions on Geoscience and Remote Sensing*, 2018.
- [34] Fei G, Fei M, Jun W, et al. Semi-Supervised Generative Adversarial Nets with Multiple Generators for SAR Image Recognition[J]. *Sensors*, 2018, 18(8):2706-.
- [35] He W, Yokoya N. Multi-Temporal Sentinel-1 and -2 Data Fusion for Optical Image Simulation [J]. *ISPRS International Journal of Geo-Information*, 2018, 7(10).
- [36] Liu J, Gong M, Qin K, et al. A Deep Convolutional Coupling Network for Change Detection Based on Heterogeneous Optical and Radar Images[J]. *IEEE Transactions on Neural Networks and Learning Systems*, 2016, PP(99):1-15.
- [37] Merkle N, Auer S, Muller R, et al. Exploring the Potential of Conditional Adversarial Networks for Optical and SAR Image Matching[J]. *IEEE Journal of Selected Topics in Applied Earth Observations and Remote Sensing*, 2018:1-10.
- [38] Ma W, Pan Z, Guo J, et al. Super-Resolution of Remote Sensing Images Based on Transferred Generative Adversarial Network[C]// IGARSS 2018 - 2018 IEEE International Geoscience and Remote Sensing Symposium. IEEE, 2018.
- [39] Arjovsky M, Chintala S, Bottou L. Wasserstein gan[J]. *arXiv preprint arXiv:1701.07875*, 2017.

- [40] Dataset: Gaofen3, China Centre for Resources Satellite Data and Application. Accessed: Jul. 2017 [Online]. Available: <http://www.cresda.com/CN/>.
- [41] Dataset: UAVSAR, NASA 2018, ASF DAAC. Accessed: Dec. 2018 [Online]. Available: <https://vertex.daac.asf.alaska.edu/>.
- [42] Cozzolino D, Parrilli S, Scarpa G, et al. Fast adaptive nonlocal SAR despeckling[J]. IEEE Geoscience and Remote Sensing Letters, 2014, 11(2): 524-528.

TABLE I
Differences between SAR images and natural optical images.

	Optical images	SAR images	SAR unique phenomena
Wave band	Visible light band	Microwave band	Discontinuity, Scintillation
Focusing mechanism	Real aperture	Coherent synthetic aperture	Speckle noise
Projection scheme	Elevation-Azimuth	Range-Azimuth	Layover, Foreshortening, Shadowing
Resolution	Proportional to range	Invariant to range	No perspective distortion
Data format	Color, Intensity	Phase, Amplitude, Polarization	Multi-channel, Complex

TABLE II
Information about the two datasets employed for experiments.

Sensor	Resolution	Polarization	Location
UAVSAR	6m	Quad-Pol	Wuhan and Hefei, China
GF3	0.51m	HH or VV	California, US

TABLE III
FIDs of different datasets.

	0.51m single-pol GF3	6m single-pol UAVSAR	10m single-pol UAVSAR	6m full-pol UAVSAR
Optical	154.8	106.4	138.4	85.6
SAR	53.0	56.0	64.7	52.8

TABLE IV
Decreasing FID with increasing the number of samples (for the case of 6m full-pol UAVSAR in Table III)

Samples	500	1000	2048	3000	4000	5000	6000	7000	8000	9000	10000
Optical	125.0	102.9	85.6	81.2	77.9	75.9	74.8	74.1	73.4	72.7	72.1
SAR	86.9	68.8	52.8	49.4	46.8	45.9	44.5	43.2	42.5	42.0	41.9

TABLE V
Result comparisons of different methods using different evaluation methods.

Evaluation Method	Sensing modalities	CycleGAN	Pix2Pix	Proposed
PSNR	Optical	14.9675	14.4686	15.5268
	SAR	15.7171	15.4978	15.8425
SSIM	Optical	0.2656	0.2317	0.2782
	SAR	0.2535	0.2194	0.2583
FID	Optical	185.3181	212.5304	154.7532
	SAR	62.1420	77.6901	53.0067

TABLE VI
FIDs of results by supervised and unsupervised learning.

	Supervised Learning	+Unsupervised Learning
Optical	107.8	88.9
SAR	58.1	41.2

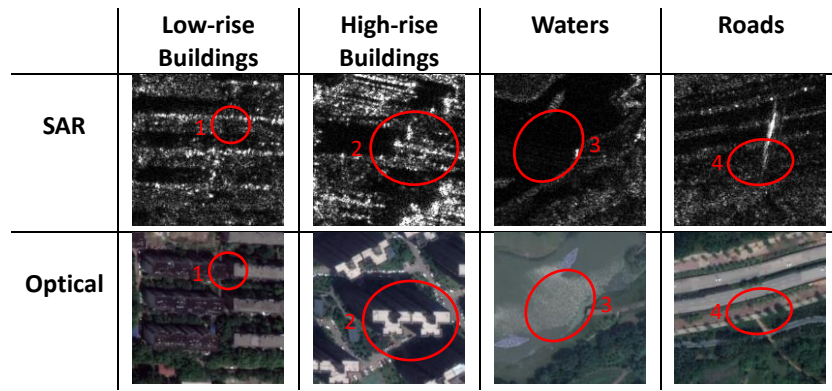


Fig. 1. Distinctions between SAR and optical remote sensing images.

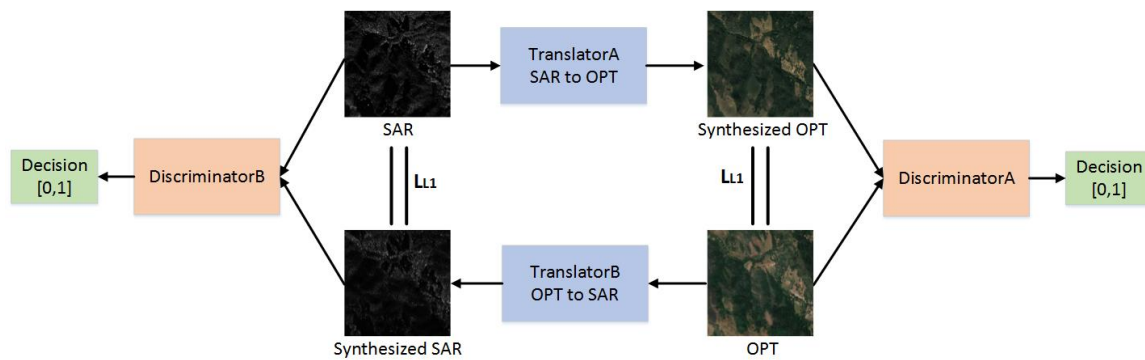


Fig. 2. Schematic diagram of the translation network during training. A pair of translators are trained together. Each translator consists of an encoder and a decoder. The two discriminators are trained separately. ‘SAR’, ‘OPT’, ‘Synthesized OPT’ and ‘Synthesized SAR’ respectively represent the true SAR image, the true optical image, the fake optical image and the fake SAR image. The two vertical lines connecting ‘SAR’ and ‘Synthesized SAR’ mean that the network should make them equal.

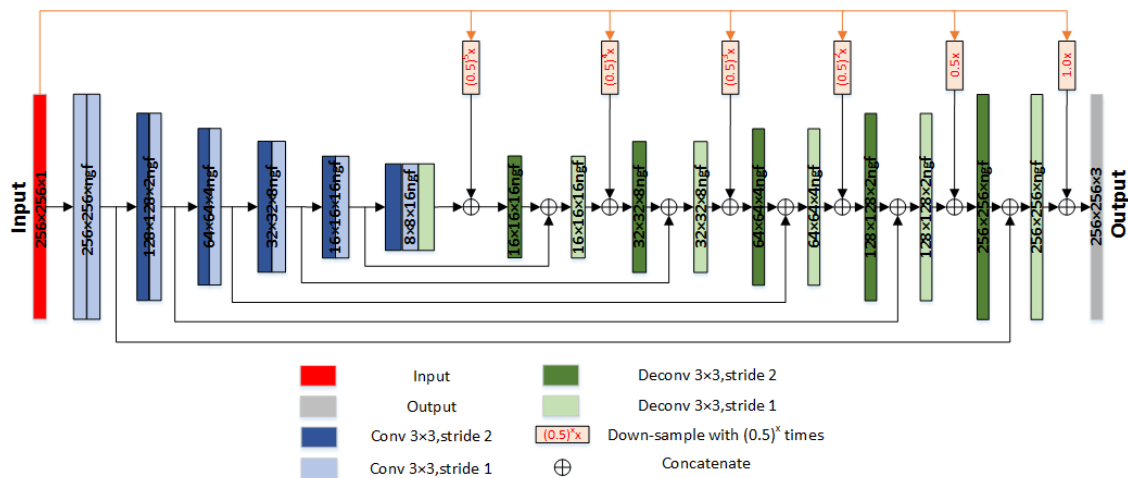


Fig. 3. Translator network architecture with cascaded-residual connections. The input data size is $256 \times 256 \times 1$ and the output data size is $256 \times 256 \times 3$. The first two numbers represent the size of the feature maps and the third number represents the channel of the feature map. The concatenation from the encoder and the input to the decoder is signified by lines with arrows.

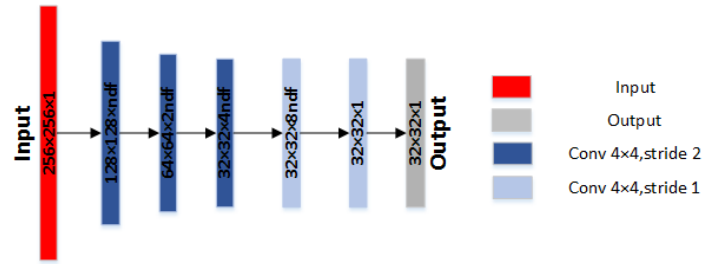


Fig. 4. Discriminator network architecture. The input data size is $256 \times 256 \times 1$ and the output probability map size is $32 \times 32 \times 1$. The first two numbers represent the size of the feature maps and the third number represents the channel of the feature map.

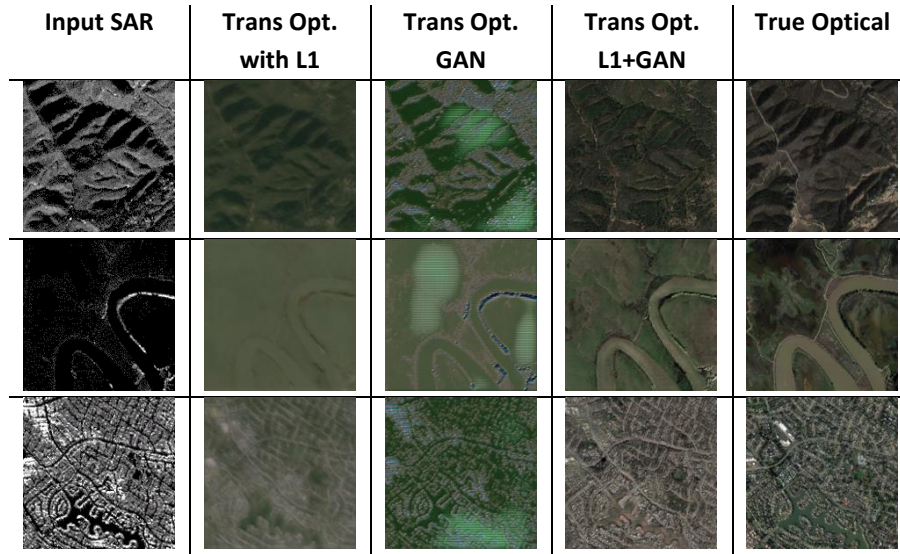


Fig. 5. Different qualities of translated optical images are induced by different losses. Each column shows results trained using different loss functions.

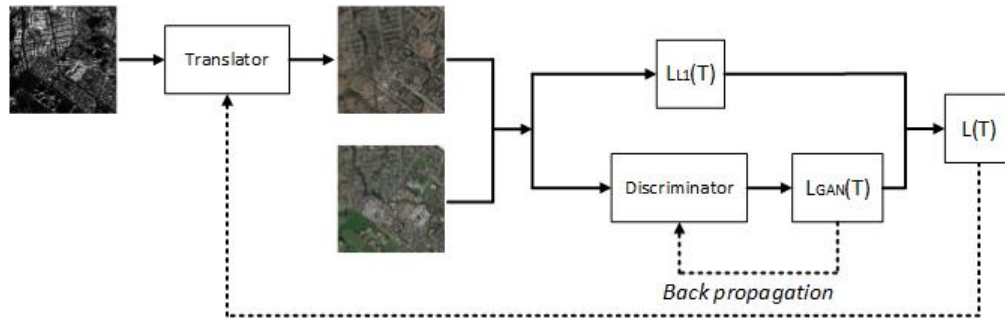


Fig. 6. The conceptual process of training the adversarial networks. The left image is the real SAR image, the upper right is the synthesized optical image and the lower right is the real optical image.

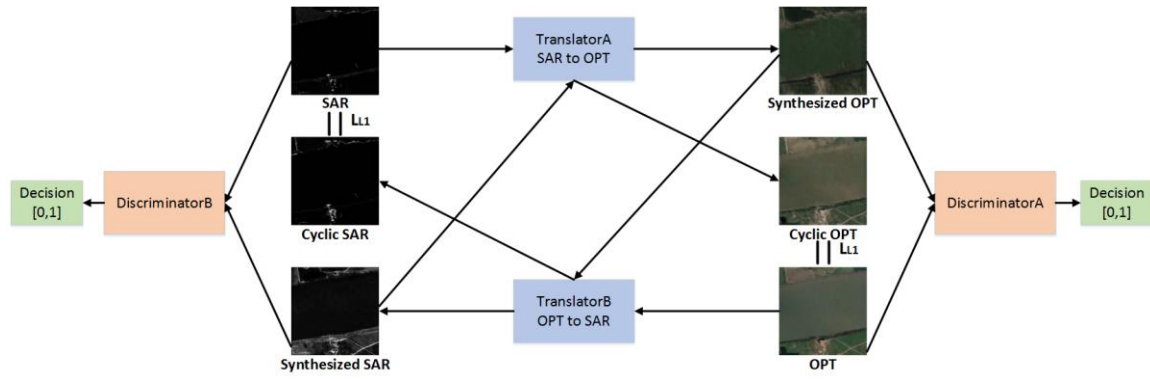


Fig.7. Modified network scheme for unsupervised learning with cyclic loops.

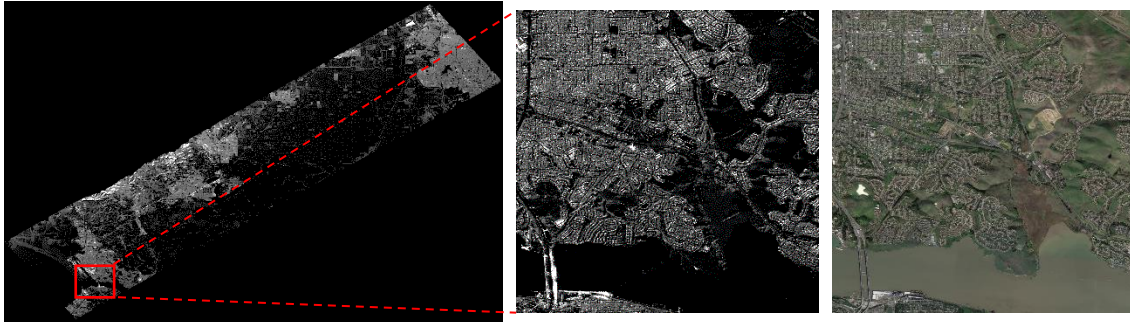


Fig. 8. (left) UAVSAR image acquired in California, US. (center) Zoomed region. (right) Corresponding optical image of the zoomed region.

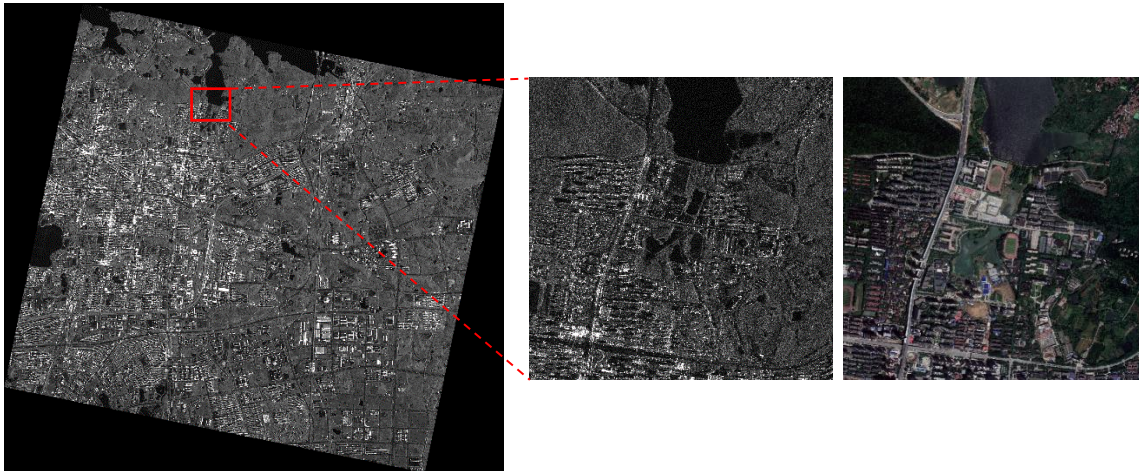


Fig. 9. (left) A large SAR image with a 0.51m resolution in Hongshan District, Wuhan City, Hubei Province, China. (center) Zoomed region. (right) Corresponding optical image of the zoomed region.

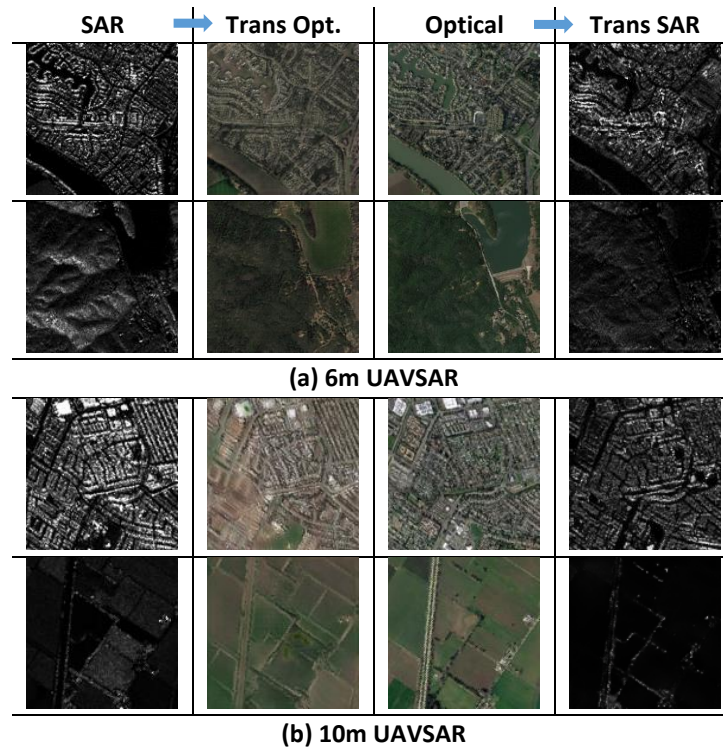


Fig. 10. Example translation images with UAVSAR (test samples). Images in each column from left to right are the real SAR image and its translated optical image, the real optical image and its translated SAR image.

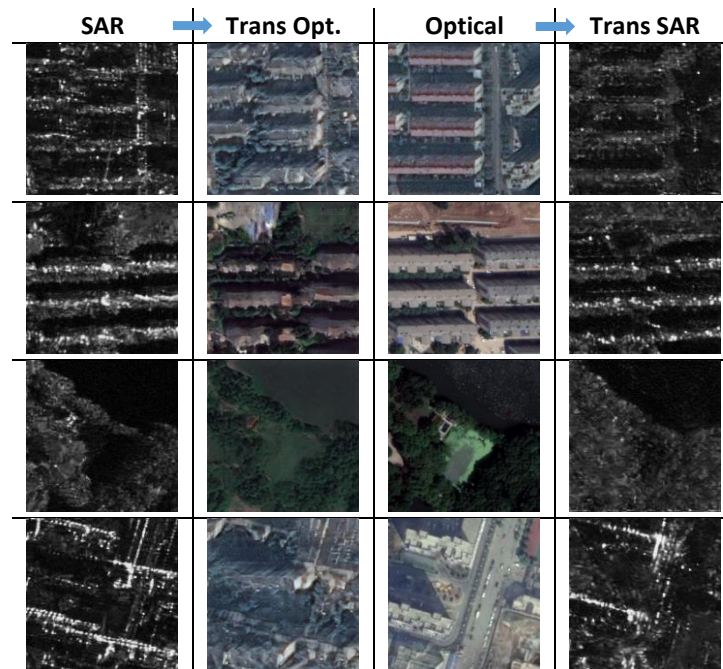


Fig. 11. Examples translation images with GF3 data. Images in each column from left to right are the real SAR image and its translated optical image, the real optical image and its translated SAR image.

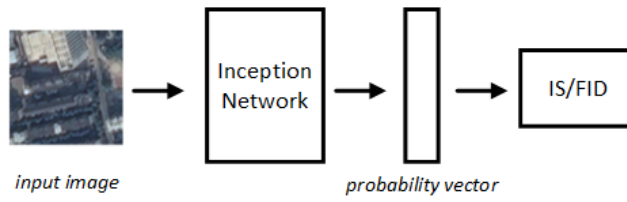


Fig.12. The conceptual process of calculating IS/FID.

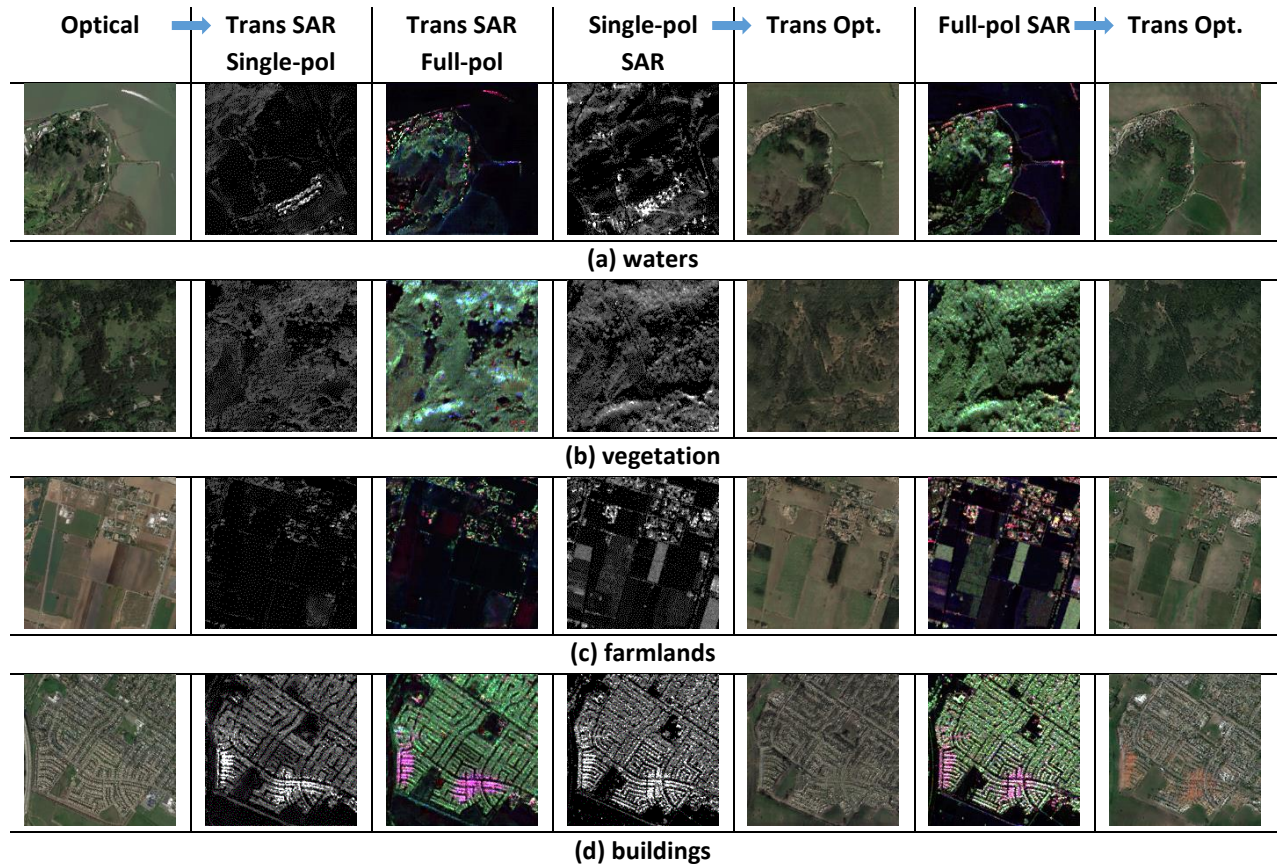


Fig. 13. Images listed above in each row are the optical ground truth and its reconstructed single-polarized SAR image and full-polarized SAR image, the single-polarized SAR ground truth and its reconstructed optical image, the full-polarized SAR ground truth and its reconstructed optical image in order. Each row lists a kind of earth surfaces.

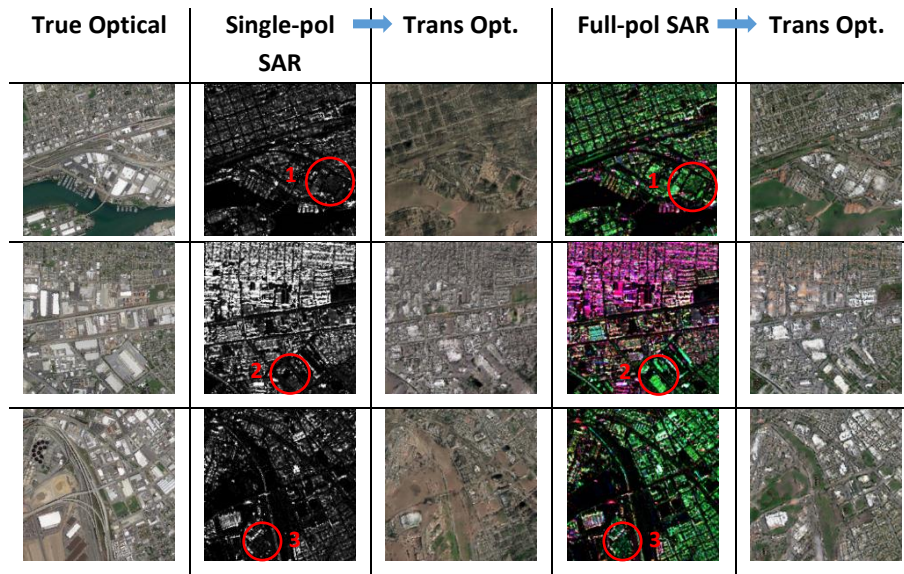


Fig. 14. Images in each column from left to right are the real optical image, the real single-pol SAR image and its translated optical image, the real Pauli image and its synthesized optical image.

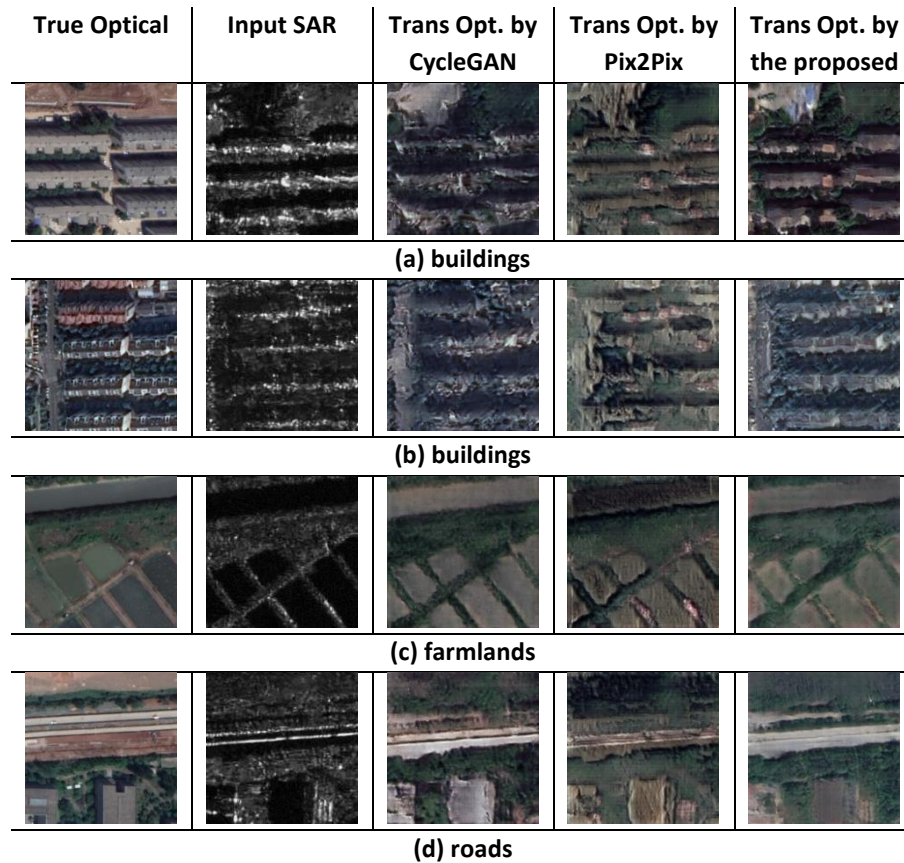


Fig. 15. Comparison of SAR-Optical translation by different methods.

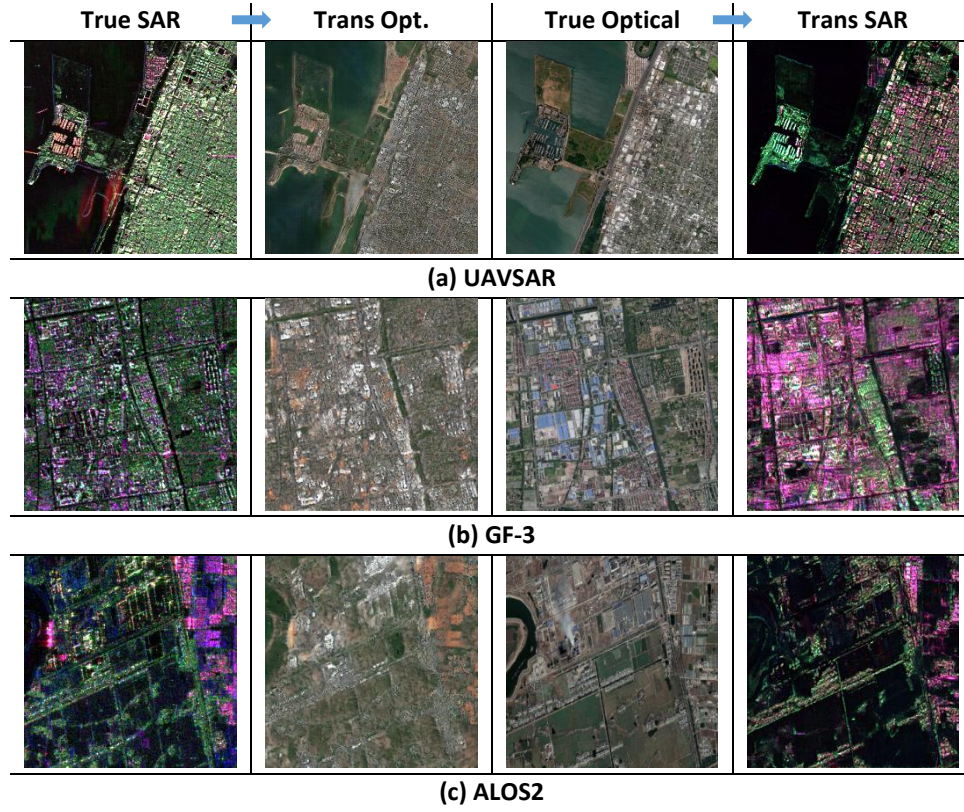


Fig. 16. Images across scenes and across sensors reconstructed by the model pre-trained with 6m UAVSAR images. Images in each row from left to right are the real SAR image and its synthesized optical image, the real optical image and its synthesized SAR image.

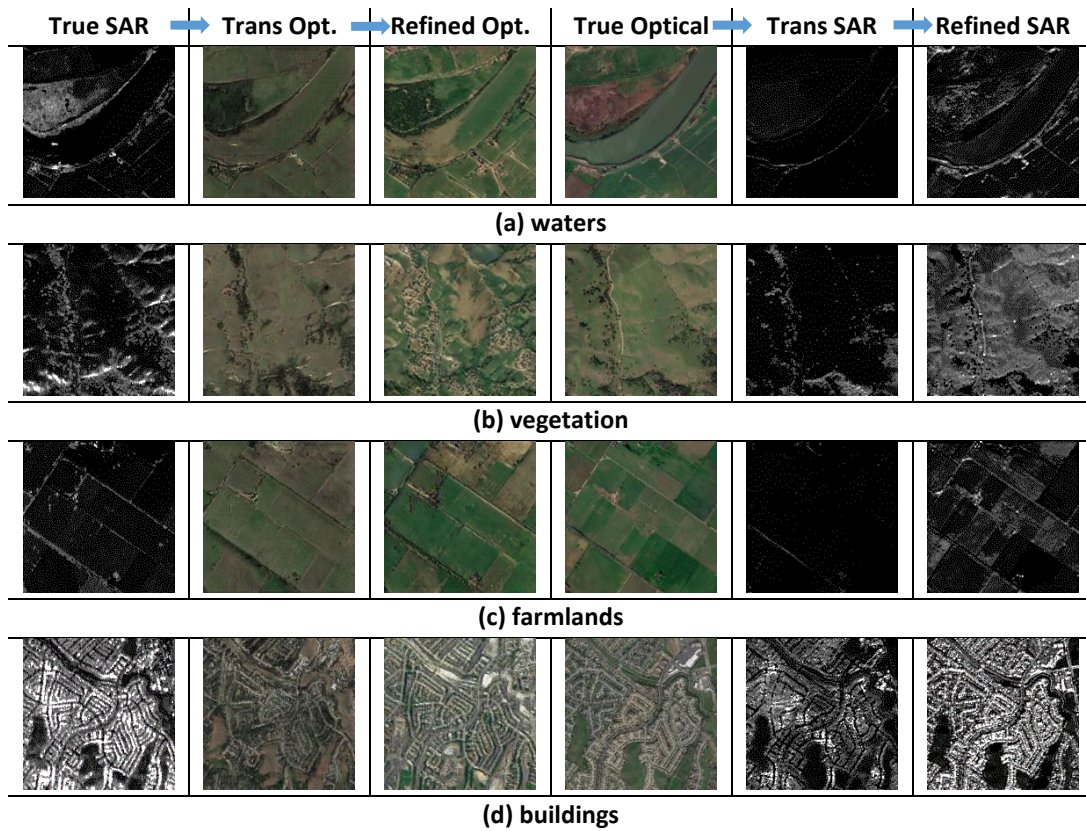


Fig. 17. Translated image further refined with unsupervised learning. Images in each column from left to right are the input SAR image, the translated optical image and the further refined version by unsupervised learning, the input optical image and its translated SAR image and the further refined version by unsupervised learning.